Geophysical Research Letters

RESEARCH LETTER
10.1029/2023GL103904

Snow Suppresses Seismic Signals From Steamboat Geyser

Mara H. Reed[1] and Michael Manga[1]

[1]Department of Earth and Planetary Science, University of California, Berkeley, CA, USA

Key Points:

- Seismic signals from Steamboat Geyser eruptions contain ground-coupled airwaves at distances up to 2.2 km
- Snow dampens airwave arrivals leading to lower apparent signal amplitudes in winter
- Interpretation of eruption signals at both geysers and volcanoes should take changing environmental factors into account

Supporting Information:

Supporting Information may be found in the online version of this article.

Correspondence to:

M. H. Reed,
mhreed@berkeley.edu

Citation:

Reed, M. H., & Manga, M. (2023). Snow suppresses seismic signals from Steamboat Geyser. *Geophysical Research Letters*, *50*, e2023GL103904. https://doi.org/10.1029/2023GL103904

Received 29 MAR 2023
Accepted 2 JUN 2023

Abstract Geyser and volcano monitoring suffer from temporal, geographic, and instrumental biases. We present a recording bias identified through multiyear monitoring of Steamboat Geyser in Yellowstone National Park, USA. Eruptions of Steamboat are the tallest of any geyser in the world and they produce broadband signals at two nearby stations in the Yellowstone National Park Seismograph Network. In winter, we observe lower eruption signal amplitudes at these seismometers. Instead of a source effect, we find that environmental conditions affect the recorded signals. Lower amplitudes for 23–45 Hz frequencies are correlated with greater snow depths at the station 340 m away from Steamboat, and we calculate an energy attenuation coefficient of 0.21 ± 0.01 dB per cm of snow. More long-term monitoring is needed at geysers to track changes over time and identify recording biases that may be missed during short, sporadic studies.

Plain Language Summary What we learn about geysers and volcanoes depends on when, where, and how we are able to monitor them. Here we present a case study of how seasonal changes affect data recorded on a seismometer, which is an instrument that measures ground motion. The world's tallest geyser, Steamboat Geyser in Yellowstone National Park, has intense eruptions that eject a mixture of water and steam. The eruptions are powerful enough to cause tiny ground motions from sound waves that begin in the air and then transfer into the ground. In the winter, we see smaller ground motions at two nearby seismometers. This might imply that Steamboat's eruptions are weaker in the winter; however, winter in Yellowstone comes with snow, and snow is good at absorbing sound wave energy. We find that smaller ground motions occur when snow depths are greater, and that the strength of ground motions should not be used to directly compare eruption intensity. Few geysers around the world are monitored with scientific equipment for long periods of time. Our result highlights the need for more of this type of monitoring so that we can identify biases that may be missed during shorter investigations.

1. Introduction

Geysers are hydrothermal features that episodically erupt a mixture of water and vapor (White, 1967). Because their physical processes and eruption dynamics bear similarities to volcanoes (Kieffer, 1984), geysers are sometimes treated as volcanic analogs with the advantage of erupting more frequently and at smaller scales (Hurwitz et al., 2021). What we learn about geysers and volcanoes is biased by when, where, and how we can monitor them. The National Academies of Sciences, Engineering, and Medicine (2017) highlighted as one of two scientific grand challenges in volcano science the need to "quantify the life cycles of volcanoes globally and overcome our current biased understanding" through expanded monitoring on the ground and from space. The same challenge exists for geyser study, where few geysers are monitored well enough to produce even basic data such as eruption timing.

Seismometers are the most commonly used instrument for monitoring volcanoes because they can detect signals related to magma interaction with rock and fluid in the subsurface (McNutt & Roman, 2015; Moran et al., 2008). They can also detect ground-coupled airwaves, generated when acoustic waves traveling through the air meet the ground at a shallow angle from horizontal, that are produced by explosive eruptions (e.g., Fee et al., 2016; Ichihara et al., 2021; Mendo-Pérez et al., 2021; Palacios et al., 2022; Smith et al., 2016). In contrast to their widespread use in volcano monitoring, seismometers are rarely used for long-term monitoring of geysers despite their usefulness for creating robust eruption interval catalogs (Eibl et al., 2020). Short-term deployments of seismic arrays, broadband instruments, and tiltmeters are more common and have been used to locate tremor and other deformation sources at multiple geysers including Old Faithful (Cros et al., 2011; Kedar et al., 1996; Vandemeulebrouck et al., 2013; Wu et al., 2017, 2019), Steamboat (Wu et al., 2021), and Lone Star (Nayak et al., 2020; Vandemeulebrouck et al., 2014) in Yellowstone, Strokkur, Iceland (Eibl et al., 2021), and El Jefe,

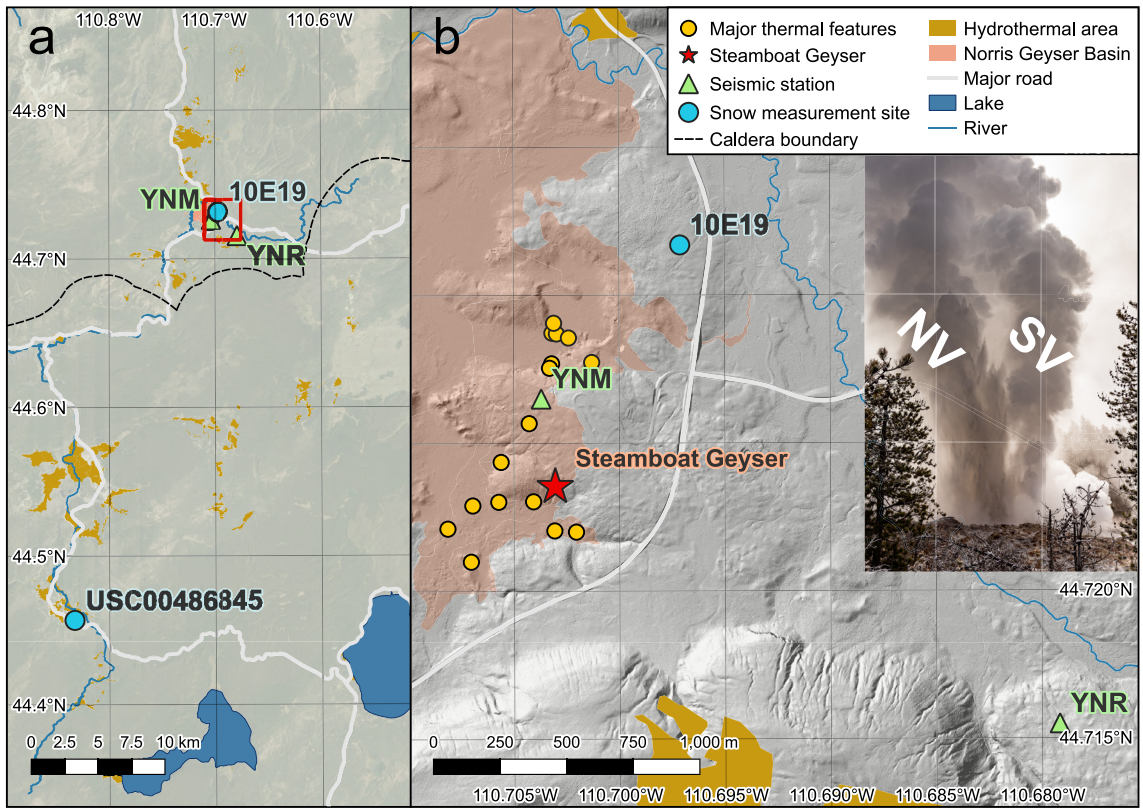

Figure 1. (a) Map showing the location of the weather station at Old Faithful relative to Norris Geyser Basin. (b) Map corresponding to the red rectangle in (a) that depicts the location of Steamboat Geyser (elevation 2,306 m), seismic stations, and the snow course. Inset photo shows Steamboat mid-eruption on 23 May 2022 with labels for the North Vent (NV) and South Vent (SV) jets.

Chile (Ardid et al., 2019), in addition to geysering wells in Calistoga, California (Rudolph et al., 2012) and Onikobe Caldera, Japan (Nishimura et al., 2006).

Here we report an unexpected recording bias at two broadband seismometers capturing the powerful eruptions of the world's tallest geyser, Steamboat Geyser in Norris Geyser Basin, Yellowstone, USA. We find that all eruptions are recorded by at least one of the instruments and that the signals likely contain a mixture of direct seismic arrivals and ground-coupled airwaves. However, the magnitude of the seismic signals varies strongly throughout the year, with much weaker signals during winter. There is a negative relationship between signal power and snow depth at frequencies >22 Hz at the closer broadband station, and we compare our observed attenuation with other studies of attenuation in snow. Finally, we discuss the implications of our findings on eruption monitoring at geysers and volcanoes and the need for more long-term monitoring that can help identify what environmental changes significantly impact seismic signal recording.

2. Data and Methods

2.1. Steamboat Geyser Eruptions

Steamboat Geyser entered an active phase, a period of frequent major eruptions occurring days to weeks apart, in March 2018 (Reed et al., 2021). Two prior active phases occurred in the 1960s and 1980s. During major eruptions, two adjacent vents participate (see inset photo in Figure 1b; Movie S1). The North Vent jet is tallest and reaches maximum heights of 85–137 m (Vander Ley, 2021) in the first few minutes. The South Vent attains ~50%–70% of the North Vent maximum. Both jets then gradually decrease in height and eventually reach a steam-dominated phase which dissipates over days. Between major eruptions, Steamboat is typically characterized by minor eruptions involving water jetting from one or both vents to <15 m.

Because its eruptions are so tall and active phases are so rare, Steamboat attracts a great deal of attention from park visitors and geyser enthusiasts. GeyserTimes, a crowdsourced database of geyser eruptions, contains a complete

catalog of eruption start times for the current active phase (GeyserTimes, 2022) as reported by in-basin observers or inferred from near-real time, publicly available monitoring data. Steamboat produces signals recorded by two broadband seismometers in the Yellowstone National Park Seismograph Network (University of Utah, 2021), a runoff channel temperature logger maintained by the Yellowstone Volcano Observatory, and a United States Geological Survey streamgage on Tantalus Creek. Here we consider the 147 eruptions that occurred from 15 March 2018 through 30 November 2021.

2.2. Snow Depth

Ground within Norris Geyser Basin can be warm enough to prevent snow accumulation; however, snow is present in cooler areas between thermal features and where trees are growing. Because there is no weather station near Steamboat that records daily snowfall, we used snow depth data from the 31.4 km distant weather station USC00486845 near Old Faithful (National Centers for Environmental Information, 2021). Snow depths were available for all but 10 eruptions. We justify use of this station by comparing its data to 16 manually recorded depths at snow course 10E19 (National Water and Climate Center, 2021) just outside of Norris Geyser Basin (Figure S1 in Supporting Information S1). The snow course depths include one measurement in April 2018 and five measurements at ∼monthly intervals in each of the three following winter seasons. There is reasonable agreement; the absolute difference between stations ranges from 0 to 20.3 cm with an average disagreement of 8.1 cm.

2.3. Seismic Data Processing

We focused on vertical motions at station YNM (2,311 m elevation) which is located in a shed ∼340 m away from Steamboat Geyser. An additional station, YNR (2,349 m elevation), detects most but not all eruptions and is located ∼2.19 km away (Figure 1). The stations each use a Nanometrics Trillium instrument with a sampling frequency of 100 Hz and a long period corner of 240 s (YNM) or 120 s (YNR). We downloaded data from the Incorporated Research Institutions for Seismology Data Management Center (IRISDMC) for both stations. YNM and YNR were operating during 91.2% and 99.3% of the eruptions, respectively. Due to its location near a busy trail, YNM is often noisy during summer days when park visitation is high. We limited our analysis to the 93 eruptions for which both YNM and YNR were operating, noise levels were low at YNM (most daytime eruptions in May–September were excluded), and a snow depth value was available.

Eruption signal start times were picked for YNM using a simple algorithm with the GeyserTimes catalog as a reference. First, we demeaned the raw data, removed the instrument response, and converted to units of velocity. We used an initial Butterworth highpass filter above 0.1 Hz to survey the data. Because there was no detectable long period signal, we then filtered the data between 5 and 45 Hz for further processing. The root mean square (RMS) vertical velocity for 10 min of noise prior to the catalog eruption start time was checked against sliding 0.5 s windows. If the RMS amplitude for the window was 20%–60% greater than the noise RMS amplitude and remained above 20% for 5 s, then the beginning of that window was selected as the start time. To obtain signal lag times for the two seismometers, we determined cross-correlation functions (Figure S2 in Supporting Information S1) using 60 s of seismic data beginning at the seismically derived eruption start times and picked the time corresponding with the maximum value in the first 30 s of the cross-correlation function. We dropped times for 32 eruptions where the maximum cross-correlation coefficient was less than an empirically derived value of 0.04.

Finally, we calculated median power spectral density (PSD) curves for one group of eruptions that occurred during periods with no snow cover ($N = 39$) and three eruption groups with different snow conditions (Figure S3 in Supporting Information S1): shallow snow cover (2.5–27.9 cm; $N = 22$), moderate snow cover (38.1–88.9 cm; $N = 25$), and deep snow cover (104.1–134.6 cm; $N = 7$). PSD curves were computed using Welch's method with a Hanning window. The locations of peak frequencies do not shift significantly over the course of individual eruptions (Figure S4 in Supporting Information S1), so we calculated the PSDs for 3-min data segments centered on the maximum vertical velocity. We obtained the median power for each frequency in the four groups and then converted to decibels referenced to 1 $(m/s)^2/Hz$. We followed the same procedure to create ambient noise PSDs for each group using 3-min windows beginning at 8 min prior to the eruption start times picked from YNM data.

3. Results

Figure 2 depicts examples of the 0.1 Hz highpass filtered eruption signals recorded at YNM. The waveforms are emergent; most reach maximum amplitude within the first few minutes and then slowly taper, though there are

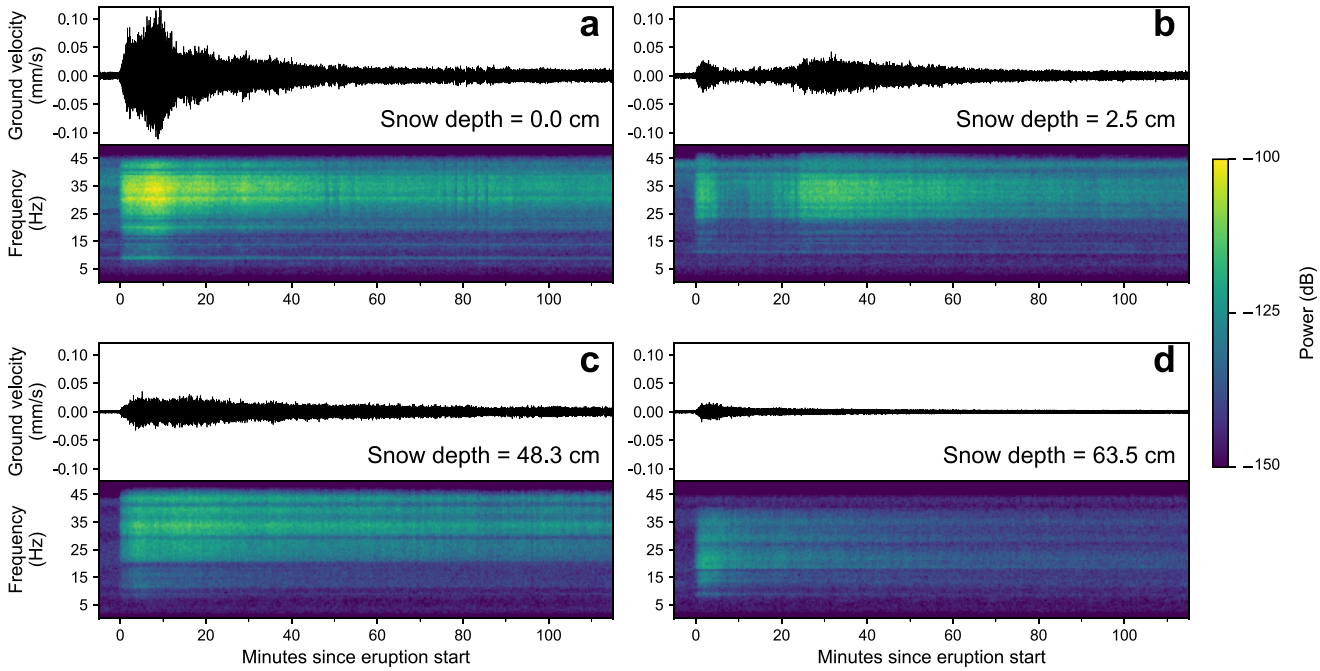

Figure 2. Example eruption seismograms and spectrograms for the YNM vertical component during Steamboat eruptions on (a) 12 September 2018, (b) 15 November 2018, (c) 8 April 2019, and (d) 1 February 2020. The records begin 5 min prior to the picked start times and have been filtered above 0.1 Hz.

exceptions (e.g., Figure 2b). We conclude that activity of the North Vent is responsible for eruptions with varying seismic amplitudes based on visual observations reported in GeyserTimes. When erupted water is blown to the east, it collects on the hillside and runs back into the North Vent which can temporarily lessen or even stop jetting (see http://geysers.org/wordpress/2018/10/20/new-crater-eruption-for-2018-october-15/ for video of this behavior). Abrupt pauses in the signal, such as those seen from 75 to 85 min into the eruption in Figure 2a, correspond to pauses in jetting from both vents.

Based on our cross-correlation analysis, there is a median lag time of 5.57 s in a range of 5.39–5.81 s for eruption signals arriving at YNR. The PSD calculations show that eruption signals recorded at both stations are broadband when there is no snow, peaking at 30–35 Hz for YNM and 15 Hz, the same frequency as a local peak in the noise, for YNR (Figure 3). Ambient noise levels decrease with increasing snow cover. At YNM, the power of eruption signal frequencies >22 Hz decreases dramatically in the moderate and deep snow bins while frequencies of 12–22 Hz remain constant across all bins. The frequency and power of the minor low frequency peak shifts slightly between groups. At YNR, all frequencies decrease in power successively for all snow groups.

Focusing just on frequencies of 23–45 Hz, we compute the signal to noise ratio (SNR) to further quantify the change in amplitude while accounting for variable noise levels. We define SNR as the RMS eruption velocity divided by the RMS noise velocity for the same 3-min windows described for the PSD calculations. The average SNR is 9.5 with a standard deviation of 3.9 for the 39 eruptions that occurred in the absence of a snow cover (Figure 4a). Despite decreasing noise, SNR still decreases with greater snow depths.

4. Discussion

4.1. Source of Seismic Waves

We hypothesize that both seismometers are recording signals dominated by ground-coupled airwaves at frequencies where power decreases with increasing snow depth. Time lags for signals arriving at YNR yield wave speeds of 318–343 m/s which correspond to the speed of sound in dry air at temperatures of −21 to 20°C. These speeds are slower than the lowest shear wave speeds of 1.19 km/s reported for sinter samples from El Tatio, Chile (Munoz-Saez et al., 2016) and 770 m/s for depths shallower than 6 m near active geysers in El Tatio (Ardid et al., 2019). The frequency distribution for signals at YNR is different than at YNM, which is likely due

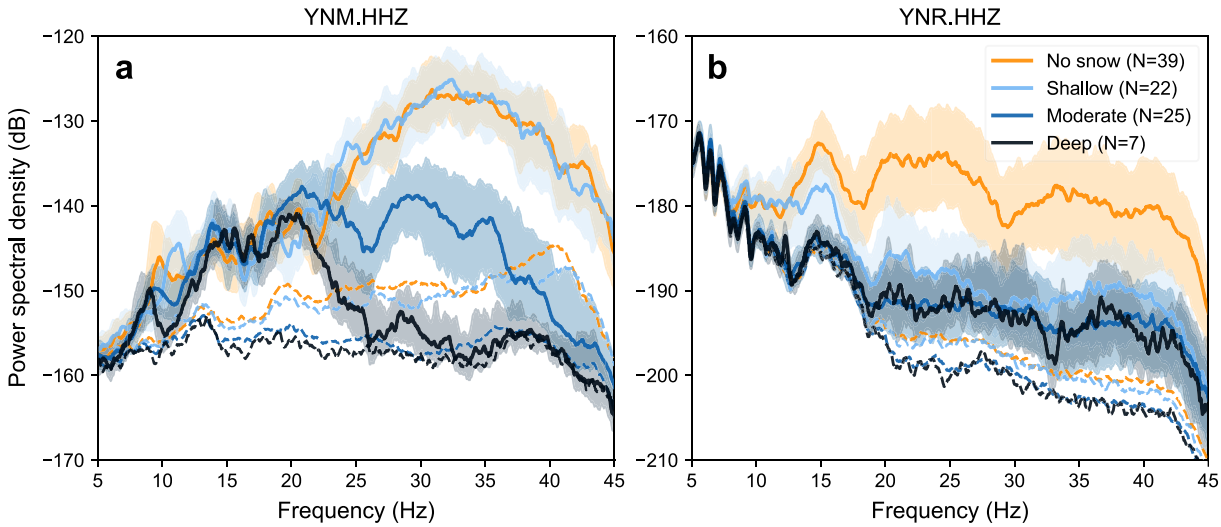

Figure 3. Pairs of median power spectral density (PSD) functions for eruptions (solid lines) and background noise (color-corresponding dashed lines) calculated for (a) YNM and (b) YNR. We also plot the interquartile range at each frequency for the eruption bins to illustrate the spread. Note the difference in vertical scales. Similar plots for horizontal motions are shown in Figure S5 in Supporting Information S1.

to the attenuating effects of topography, vegetation, and wind on sound waves traveling through the air (e.g., Attenborough, 2002; Piercy et al., 1977). Volcanoes and fumaroles are known to produce low frequency jet noise that arises from large- and fine-scale turbulence (Fee et al., 2013; Gestrich et al., 2021; Lamb et al., 2022; Matoza et al., 2009; McKee et al., 2017; Taddeucci et al., 2014; Woulff & McGetchin, 1976). Steamboat eruptions produce a low roar that is comparable to that of a jet engine (Movie S1), and given that the much smaller eruptions of Lone Star Geyser are thought to generate jet noise (Quezada-Reyes, 2012), it is possible that jet noise is the origin of acoustic waves at Steamboat.

It is unclear why the 12–22 Hz band on the vertical component of YNM remains at the same power regardless of snow level. Since the emergent signal at these frequencies (especially below ~20 Hz) is delayed by tens of seconds when compared to higher frequencies (Figure S6 in Supporting Information S1), we hypothesize that a different process might transmit energy directly through the ground but attenuate before reaching YNR. We rule out erupted water droplet impacts as a source because both water drip experiments (Dean, 2017) and observations from co-located seismometers and disdrometers (Bakker et al., 2022) show that noise from water droplets is

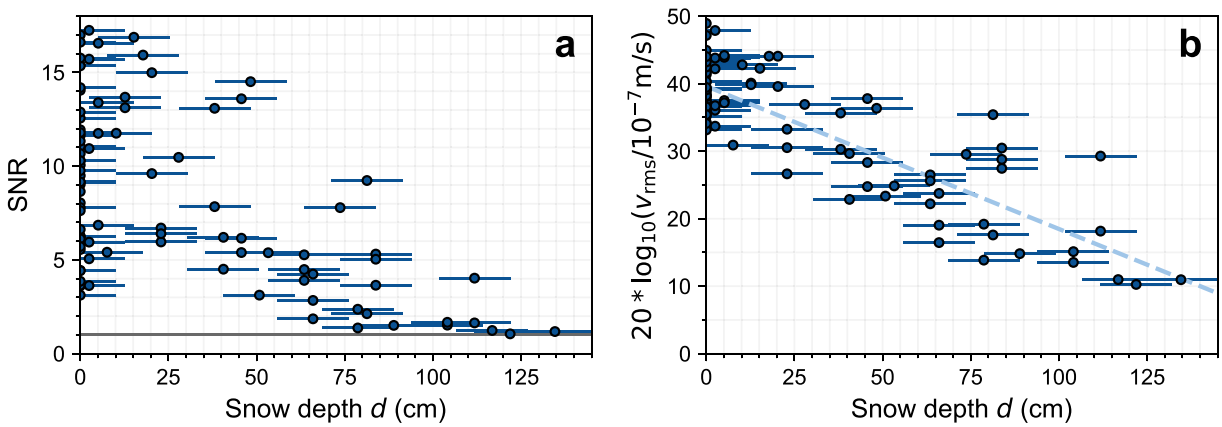

Figure 4. (a) SNR versus snow depth, d, for YNM vertical velocity at frequencies of 23–45 Hz. SNR is calculated for the vertical component data by dividing the RMS velocity of a 3-min window centered on the maximum velocity, v_{rms}, by the RMS velocity of noise in the window 5–8 min prior to the eruption. The horizontal gray line is plotted at SNR = 1. (b) Relationship between v_{rms} and d where v_{rms} is expressed in decibels referenced to 10^{-7} m/s. We use a nonlinear least squares regression to fit a line and obtain an attenuation coefficient of 0.21 ± 0.01 dB/cm. Error bars extend to ±10.2 cm, the standard deviation of differences between the Norris and Old Faithful snow depth measurements, for non-summer eruptions.

concentrated at frequencies >50 Hz. Furthermore, Bakker et al. (2022) estimate that 90% of rainfall signal comes from droplets impacting within 5–25 m of the seismometer, well below the 340 m distance between YNM and Steamboat. Hydrothermal tremor, or subsurface bubble collapse and nucleation, is concentrated in the 1–5 Hz band at Steamboat and decreases in amplitude at eruption initiation (Wu et al., 2021), so this would also not be the source of direct seismic arrivals.

The 12–22 Hz band may instead be analogous to the "high frequency wave trains" identified by Kieffer (1984) at Old Faithful and other jetting geysers in Yellowstone. Kieffer (1984) hypothesized that these signals occur due to pressure perturbations through liquid water in the conduit; once an eruption becomes steam-dominated, this signal disappears. This is a plausible source at Steamboat because frequencies below ∼23 Hz decay more quickly than higher frequencies in our data (Figure S4 in Supporting Information S1) and the steam fraction in the water column generally increases over the course of Steamboat's eruptions. To confirm this, future work might compare 12–22 Hz signal power with steam fraction in the jet, which can be estimated from video (Karlstrom et al., 2013).

4.2. Attenuation in Snow

We attribute the dampened wintertime signals to snow accumulation rather than a seasonal change in eruption intensity or weather effect. Though the presence of wind can create a negative sound speed gradient, causing upward refraction and reduced sound levels upwind from the source (Attenborough, 2002), we do not find that wind is a major factor in this case. Data from an eddy covariance tower installed at the northern end of Norris Geyser Basin between 2018 and 2020 (Lewicki & Dobeck, 2020) show that winds at Norris come primarily from the southwest and north, the latter of which blows against sound radiating from Steamboat toward YNM. However, there is little correlation between wind speeds and SNR for the 58 eruptions with available data ($r = -0.12$; Figure S7 in Supporting Information S1).

Biot's (1956a, 1956b) model for propagation of elastic waves in a porous, fluid-saturated medium predicts that attenuation increases as snow depth and signal frequency increase and snow density decreases (Johnson, 1982). We follow the fitting method of Capelli et al. (2016) to model the snow's effect on ground motion, assuming that $20\log_{10}(v_{\mathrm{rms}}) \sim e^{-\alpha d}$, where v_{rms} is the RMS eruption velocity, α is the energy attenuation coefficient, and d is the snow depth. We use a least squares method to obtain a linear fit for the snow depth and decibel-converted RMS velocity data and obtain $\alpha = 0.21 \pm 0.01$ dB/cm (Figure 4b). Though we have no data on the physical properties of the snow, we generally see a larger decrease in power for high frequencies at YNM and YNR which is consistent with this model (Figure 3). One caveat is that the PSD for the shallow snow group is nearly identical to bare conditions at YNM. The shallow group distribution is skewed toward depths of just a few cm (Figure S3 in Supporting Information S1), but this explanation for the lack of attenuation at YNM is inconsistent with observed attenuation at YNR. A more likely explanation is that when temperatures are warmer in late fall and early spring, snow at Norris melts faster than outside the geyser basin due to higher heat flux from the ground. Colder winter air and the presence of a deeper snowpack would suppress this effect.

Sound absorption due to snow has long been documented (e.g., Kaye & Evans, 1939), but few studies investigate signal attenuation at low frequencies. Our α value of 0.21 dB/cm is similar to a theoretical attenuation coefficient (∼0.1 dB/cm at 40 Hz) for Biot slow waves, dilatational waves that transmit through pore fluids, in snow and an extrapolated coefficient (∼0.2 dB/cm at frequencies on the order of 10 Hz) based on laboratory measurements performed with signals >8 kHz (Capelli et al., 2016). Other field experiments, however, found somewhat higher values for energy attenuation: 3.6 dB/cm for 5–500 Hz with seismometers buried 25 cm in soil recording coupled airwaves from a pistol shot (Albert & Orcutt, 1989) and 2–3 dB/cm for 150–200 Hz with accelerometers embedded 6–54 cm deep in snowpack responding to directed gas explosions (Simioni et al., 2017). These differences are expected because the frequencies recorded in these experiments extended to a few hundred Hz.

We emphasize that there are limitations in our ability to quantify energy attenuation. Steamboat is a continuous source of variable intensity which makes eruptions difficult to compare. Our snow depth measurements come from a weather station >30 km away, so the exact depth at the seismometers is unknown, and we have no information about snowpack porosity, density, or other parameters that affect attenuation (Johnson, 1982). However, the depth measurements from Old Faithful correlate reasonably well with the monthly measurements from the snow course near Norris (Figure S1 in Supporting Information S1). Finally, we do not explore the potential effect of changing soil properties due to a lack of data. Freeze-thaw cycles cause seasonal changes in seismic

velocity (James et al., 2019; Lindner et al., 2021; Steinmann et al., 2021) and increased soil moisture content can amplify seismic waves (Jefferson et al., 1998; Taylor et al., 2014). More work is needed to quantify any effect of these properties on air-ground coupling.

4.3. Implications for Geyser and Volcano Monitoring

Though snow loading is known to influence relative seismic velocity at volcanoes (Cannata et al., 2017; Hotovec-Ellis et al., 2014), we found only one report of signal attenuation due to snow in existing volcano literature. At Villarrica, Chile, sound levels declined by ∼5 orders of magnitude over 50 days as snow accumulated on infrasound sensors (Richardson et al., 2014). In this case, the seismometers did not record a decrease in amplitude, but the seismic signals were dominated by direct seismic arrivals. Our findings have implications for studies interpreting seismo-acoustic data at volcanoes where snow is present on the path between source and monitoring equipment, as the attenuating effect might be misinterpreted as a change in source activity. Additionally, varying snow depths at different stations will produce varying attenuation.

This recording bias would not have been identified without long-term monitoring. The existing seismic network in Yellowstone was not built to detect geyser activity and most geysers' eruptions do not produce ground motion above noise levels at large distances. Giantess Geyser in the Upper Geyser Basin is the only other geyser known to produce signals at a Yellowstone network station (YFT at ∼1.5 km distance). Especially in areas with many active geysers, future monitoring deployments must be designed to both detect and correctly attribute signals to different geysers. Infrasound monitoring, which is increasingly used at volcanoes (De Angelis et al., 2019; Fee & Matoza, 2013; Johnson & Ripepe, 2011; Watson et al., 2022), may help address this challenge. Analysis of data from a week-long deployment of an infrasound array in the Lower Geyser Basin, Yellowstone readily discriminated bursting activity from nearby fountain-type geysers but did not register jetting from cone-type geysers (Johnson et al., 2013). Jetting can still be detected if it is both tall and energetic: Steamboat's eruptions have been recorded through targeted infrasound monitoring (Holahan et al., 2021) as have Old Faithful's and Lone Star's (Johnson et al., 2013). Pilot studies should be conducted for planned infrasound arrays and/or seismometers in multiple seasons to ensure signals can be recorded year-round.

5. Conclusions

We analyzed seismic data from Steamboat Geyser eruptions and found that snow depth negatively correlates with signal amplitude. At a station 340 m distant from Steamboat, attenuation occurs at frequencies >22 Hz where ground-coupled airwaves dominate the signal. We calculate an energy attenuation coefficient of 0.21 ± 0.01 dB/cm. Steamboat has powerful eruptions; for less energetic geysers, deep snow could lead to eruptions being missed in seismic data. Changing snow depth should be considered when modeling eruption parameters using seismic amplitude if the signal contains ground-coupled airwaves. Long-term monitoring is required to track geyser activity over time and identify environmental conditions that introduce recording biases.

Conflict of Interest

M. H. Reed volunteers as a scientific advisor for GeyserTimes.

Data Availability Statement

Data from the Yellowstone National Park Seismograph Network can be downloaded from the IRISDMC (see http://ds.iris.edu/mda/WY/ for availability), and we acknowledge the use of ObsPy v1.2.2 (Krischer et al., 2015; The ObsPy Development Team, 2020) for seismic data retrieval and processing. Daily summaries of weather data at Old Faithful, including snow depth, are available from https://www.ncdc.noaa.gov/cdo-web/datasets/GHCND/stations/GHCND:USC00486845/detail while data from the snow course at Norris can be accessed at https://wcc.sc.egov.usda.gov/reportGenerator/. Wind data comes from https://doi.org/10.5066/P9AKQFGV. The catalog of eruptions from GeyserTimes may be generated at https://geysertimes.org/retrieve.php by searching primary entries for Steamboat Geyser for the period 15 March 2018 through 30 November 2021. The GIS data used for Figure 1 can be downloaded from https://www.wsgs.wyo.gov/pubs-maps/gis.aspx and https://irma.nps.gov/DataStore/Reference/Profile/1038193.

Acknowledgments
We thank Maggie Holahan and Zach Keskinen for productive conversations about infrasound attenuation in snow. Oliver Lamb and two anonymous reviewers provided comments that greatly improved the manuscript. We also thank geyser enthusiasts for sharing observations and the University of Utah for maintaining the seismometers. Financial support came from NSF Grant EAR2116573 and CIFAR Earth 4D.

References

Albert, D. G., & Orcutt, J. A. (1989). Observations of low-frequency acoustic-to-seismic coupling in the summer and winter. *Journal of the Acoustical Society of America*, *86*(1), 352–359. https://doi.org/10.1121/1.398351

Ardid, A., Vera, E., Kelly, C., Manga, M., Munoz-Saez, C., Maksymowicz, A., & Ortega-Culaciati, F. (2019). Geometry of geyser plumbing inferred from ground deformation. *Journal of Geophysical Research: Solid Earth*, *124*(1), 1072–1083. https://doi.org/10.1029/2018JB016454

Attenborough, K. (2002). Sound propagation close to the ground. *Annual Review of Fluid Mechanics*, *34*(1), 51–82. https://doi.org/10.1146/annurev.fluid.34.081701.143541

Bakker, M., Legout, C., Gimbert, F., Nord, G., Boudevillain, B., & Freche, G. (2022). Seismic modelling and observations of rainfall. *Journal of Hydrology*, *610*, 127812. https://doi.org/10.1016/j.jhydrol.2022.127812

Biot, M. A. (1956a). Theory of propagation of elastic waves in a fluid-saturated porous solid. I. Low-frequency range. *Journal of the Acoustical Society of America*, *28*(2), 168–178. https://doi.org/10.1121/1.1908239

Biot, M. A. (1956b). Theory of propagation of elastic waves in a fluid-saturated porous solid. II. Higher frequency range. *Journal of the Acoustical Society of America*, *28*(2), 179–191. https://doi.org/10.1121/1.1908241

Cannata, A., Cannavò, F., Montalto, P., Ercoli, M., Mancinelli, P., Pauselli, C., & Leto, G. (2017). Monitoring crustal changes at volcanoes by seismic noise interferometry: Mt. Etna case of study. *Journal of Volcanology and Geothermal Research*, *337*, 165–174. https://doi.org/10.1016/j.jvolgeores.2017.03.023

Capelli, A., Kapil, J. C., Reiweger, I., Or, D., & Schweizer, J. (2016). Speed and attenuation of acoustic waves in snow: Laboratory experiments and modeling with Biot's theory. *Cold Regions Science and Technology*, *125*, 1–11. https://doi.org/10.1016/j.coldregions.2016.01.004

Cros, E., Roux, P., Vandemeulebrouck, J., & Kedar, S. (2011). Locating hydrothermal acoustic sources at Old Faithful Geyser using matched field processing. *Geophysical Journal International*, *187*(1), 385–393. https://doi.org/10.1111/j.1365-246X.2011.05147.x

Dean, T. (2017). The seismic signature of rain. *Geophysics*, *82*(5), P53–P60. https://doi.org/10.1190/geo2016-0421.1

De Angelis, S., Diaz-Moreno, A., & Zuccarello, L. (2019). Recent developments and applications of acoustic infrasound to monitor volcanic emissions. *Remote Sensing*, *11*(11), 1302. https://doi.org/10.3390/rs11111302

Eibl, E. P. S., Hainzl, S., Vesely, N. I. K., Walter, T. R., Jousset, P., Hersir, G. P., & Dahm, T. (2020). Eruption interval monitoring at Strokkur Geyser, Iceland. *Geophysical Research Letters*, *47*(1), e2019GL085266. https://doi.org/10.1029/2019GL085266

Eibl, E. P. S., Müller, D., Walter, T. R., Allahbakhshi, M., Jousset, P., Hersir, G. P., & Dahm, T. (2021). Eruptive cycle and bubble trap of Strokkur Geyser, Iceland. *Journal of Geophysical Research: Solid Earth*, *126*(4), e2020JB020769. https://doi.org/10.1029/2020JB020769

Fee, D., Haney, M., Matoza, R., Szuberla, C., Lyons, J., & Waythomas, C. (2016). Seismic envelope-based detection and location of ground-coupled airwaves from volcanoes in Alaska. *Bulletin of the Seismological Society of America*, *106*(3), 1024–1035. https://doi.org/10.1785/0120150244

Fee, D., & Matoza, R. S. (2013). An overview of volcano infrasound: From Hawaiian to Plinian, local to global. *Journal of Volcanology and Geothermal Research*, *249*, 123–139. https://doi.org/10.1016/j.jvolgeores.2012.09.002

Fee, D., Matoza, R. S., Gee, K. L., Neilsen, T. B., & Ogden, D. E. (2013). Infrasonic crackle and supersonic jet noise from the eruption of Nabro Volcano, Eritrea. *Geophysical Research Letters*, *40*(16), 4199–4203. https://doi.org/10.1002/grl.50827

Gestrich, J. E., Fee, D., Matoza, R. S., Lyons, J. J., & Ruiz, M. C. (2021). Fitting jet noise similarity spectra to volcano infrasound data. *Earth and Space Science*, *8*(11), e2021EA001894. https://doi.org/10.1029/2021EA001894

GeyserTimes. (2022). [Steamboat Geyser eruptions for 1 March 2018 through 30 November 2021]. [Dataset]. Retrieved from https://geysertimes.org/retrieve.php

Holahan, M., Johnson, J. B., Bosa, A., & Satterwhite, T. (2021). Characterizing a year of Steamboat Geyser's activity using dual infrasound arrays in Yellowstone National Park. Presented at the AGU Fall Meeting 2021, AGU. Retrieved from https://agu.confex.com/agu/fm21/meetingapp.cgi/Paper/900786

Hotovec-Ellis, A. J., Gomberg, J., Vidale, J. E., & Creager, K. C. (2014). A continuous record of intereruption velocity change at Mount St. Helens from coda wave interferometry. *Journal of Geophysical Research: Solid Earth*, *119*(3), 2199–2214. https://doi.org/10.1002/2013JB010742

Hurwitz, S., Manga, M., Campbell, K. A., Munoz-Saez, C., & Eibl, E. P. S. (2021). Why study geysers? *Eos*, *102*. https://doi.org/10.1029/2021EO161365

Ichihara, M., Yamakawa, K., & Muramatsu, D. (2021). A simple method to evaluate the air-to-ground coupling efficiency: A tool helping the assessment of seismic/infrasonic energy partitioning during an eruption. *Earth Planets and Space*, *73*(180), 180. https://doi.org/10.1186/s40623-021-01510-4

James, S. R., Knox, H. A., Abbott, R. E., Panning, M. P., & Screaton, E. J. (2019). Insights into permafrost and seasonal active-layer dynamics from ambient seismic noise monitoring. *Journal of Geophysical Research: Earth Surface*, *124*(7), 1798–1816. https://doi.org/10.1029/2019JF005051

Jefferson, R. D., Steeples, D. W., Black, R. A., & Carr, T. (1998). Effects of soil-moisture content on shallow-seismic data. *Geophysics*, *63*(4), 1357–1362. https://doi.org/10.1190/1.1444437

Johnson, J. B. (1982). On the application of Biot's theory to acoustic wave propagation in snow. *Cold Regions Science and Technology*, *6*(1), 49–60. https://doi.org/10.1016/0165-232X(82)90044-1

Johnson, J. B., Anderson, J. F., Anthony, R. E., & Sciotto, M. (2013). Detecting geyser activity with infrasound. *Journal of Volcanology and Geothermal Research*, *256*, 105–117. https://doi.org/10.1016/j.jvolgeores.2013.02.016

Johnson, J. B., & Ripepe, M. (2011). Volcano infrasound: A review. *Journal of Volcanology and Geothermal Research*, *206*(3), 61–69. https://doi.org/10.1016/j.jvolgeores.2011.06.006

Karlstrom, L., Hurwitz, S., Sohn, R., Vandemeulebrouck, J., Murphy, F., Rudolph, M. L., et al. (2013). Eruptions at Lone Star Geyser, Yellowstone National Park, USA: 1. Energetics and eruption dynamics. *Journal of Geophysical Research: Solid Earth*, *118*(8), 4048–4062. https://doi.org/10.1002/jgrb.50251

Kaye, G. W. C., & Evans, E. J. (1939). Sound absorption of snow. *Nature*, *143*(3611), 80. https://doi.org/10.1038/143080a0

Kedar, S., Sturtevant, B., & Kanamori, H. (1996). The origin of harmonic tremor at Old Faithful Geyser. *Nature*, *379*(6567), 708–711. https://doi.org/10.1038/379708a0

Kieffer, S. W. (1984). Seismicity at Old Faithful Geyser: An isolated source of geothermal noise and possible analogue of volcanic seismicity. *Journal of Volcanology and Geothermal Research*, *22*(1), 59–95. https://doi.org/10.1016/0377-0273(84)90035-0

Krischer, L., Megies, T., Barsch, R., Beyreuther, M., Lecocq, T., Caudron, C., & Wassermann, J. (2015). ObsPy: A bridge for seismology into the scientific Python ecosystem. *Computational Science & Discovery*, *8*(1), 014003. https://doi.org/10.1088/1749-4699/8/1/014003

Lamb, O. D., Gestrich, J. E., Barnie, T. D., Jónsdóttir, K., Ducrocq, C., Shore, M. J., et al. (2022). Acoustic observations of lava fountain activity during the 2021 Fagradalsfjall eruption, Iceland. *Bulletin of Volcanology*, *84*(11), 96. https://doi.org/10.1007/s00445-022-01602-3

Lewicki, J. L., & Dobeck, L. M. (2020). Long-term gas and heat emissions measurements, Norris Geyser Basin, Yellowstone National Park. [Dataset]. U.S. Geological Survey. https://doi.org/10.5066/P9AKQFGV

Lindner, F., Wassermann, J., & Igel, H. (2021). Seasonal freeze-thaw cycles and permafrost degradation on Mt. Zugspitze (German/Austrian Alps) revealed by single-station seismic monitoring. *Geophysical Research Letters*, *48*(18), e2021GL094659. https://doi.org/10.1029/2021GL094659

Matoza, R. S., Fee, D., Garcés, M. A., Seiner, J. M., Ramón, P. A., & Hedlin, M. A. H. (2009). Infrasonic jet noise from volcanic eruptions. *Geophysical Research Letters*, *36*(8), L08303. https://doi.org/10.1029/2008GL036486

McKee, K., Fee, D., Yokoo, A., Matoza, R. S., & Kim, K. (2017). Analysis of gas jetting and fumarole acoustics at Aso Volcano, Japan. *Journal of Volcanology and Geothermal Research*, *340*, 16–29. https://doi.org/10.1016/j.jvolgeores.2017.03.029

McNutt, S. R., & Roman, D. C. (2015). Volcanic seismicity. In H. Sigurdsson, B. Houghton, S. R. McNutt, H. Rymer, & J. Stix (Eds.), *The encyclopedia of volcanoes* (2nd ed., pp. 1011–1034). Academic Press. https://doi.org/10.1016/B978-0-12-385938-9.00059-6

Mendo-Pérez, G., Arciniega-Ceballos, A., Matoza, R. S., Rosado-Fuentes, A., Sanderson, R. W., & Chouet, B. A. (2021). Ground-coupled airwaves template match detection using broadband seismic records of explosive eruptions at Popocatépetl volcano, Mexico. *Journal of Volcanology and Geothermal Research*, *419*, 107378. https://doi.org/10.1016/j.jvolgeores.2021.107378

Moran, S. C., Freymueller, J. T., LaHusen, R. G., McGee, K. A., Poland, M. P., Power, J. A., et al. (2008). Instrumentation recommendations for volcano monitoring at U.S. volcanoes under the National volcano early warning system (Scientific investigations report 2008-5114). *U.S. Geological Survey*. https://doi.org/10.3133/sir20085114

Munoz-Saez, C., Saltiel, S., Manga, M., Nguyen, C., & Gonnermann, H. (2016). Physical and hydraulic properties of modern sinter deposits: El Tatio, Atacama. *Journal of Volcanology and Geothermal Research*, *325*, 156–168. https://doi.org/10.1016/j.jvolgeores.2016.06.026

National Academies of Sciences, Engineering, and Medicine. (2017). *Volcanic eruptions and their repose, unrest, precursors, and timing*. The National Academies Press. https://doi.org/10.17226/24650

National Centers for Environmental Information. (2021). [Daily summaries of precipitation and temperature extrema for station USC00486845 at Old Faithful, Wyoming, USA]. [Dataset]. Retrieved from https://www.ncdc.noaa.gov/cdo-web/datasets/GHCND/stations/GHCND:USC00486845/detail

National Water and Climate Center. (2021). [Snow depth measurements at snow course 10E19]. [Dataset]. Retrieved from https://wcc.sc.egov.usda.gov/reportGenerator/

Nayak, A., Manga, M., Hurwitz, S., Namiki, A., & Dawson, P. B. (2020). Origin and properties of hydrothermal tremor at Lone Star Geyser, Yellowstone National Park, USA. *Journal of Geophysical Research: Solid Earth*, *125*(12), e2020JB019711. https://doi.org/10.1029/2020JB019711

Nishimura, T., Ichihara, M., & Ueki, S. (2006). Investigation of the Onikobe geyser, NE Japan, by observing the ground tilt and flow parameters. *Earth Planets and Space*, *58*(6), e21–e24. https://doi.org/10.1186/BF03351967

Palacios, P. B., Mader, H. M., Kendall, J., & Yepes, H. A. (2022). Seismic tremor location of ten large paroxysmal eruptions of Tungurahua volcano, Ecuador. *Geophysical Journal International*, *233*(2), 1460–1483. https://doi.org/10.1093/gji/ggac523

Piercy, J. E., Embleton, T. F. W., & Sutherland, L. C. (1977). Review of noise propagation in the atmosphere. *Journal of the Acoustical Society of America*, *61*(6), 1403–1418. https://doi.org/10.1121/1.381455

Quezada-Reyes, A. (2012). Characterization of some Yellowstone Geysers' eruptions using infrasound [Master's thesis, New Mexico Institute of Mining and Technology]. Retrieved from http://www.ees.nmt.edu/outside/alumni/papers/2012i_quezada-reyes_a.pdf

Reed, M. H., Munoz-Saez, C., Hajimirza, S., Wu, S.-M., Barth, A., Girona, T., et al. (2021). The 2018 reawakening and eruption dynamics of Steamboat Geyser, the world's tallest active geyser. *Proceedings of the National Academy of Sciences*, *118*(2). https://doi.org/10.1073/pnas.2020943118

Richardson, J. P., Waite, G. P., & Palma, J. L. (2014). Varying seismic-acoustic properties of the fluctuating Lava Lake at Villarrica volcano, Chile. *Journal of Geophysical Research: Solid Earth*, *119*(7), 5560–5573. https://doi.org/10.1002/2014JB011002

Rudolph, M. L., Manga, M., Hurwitz, S., Johnston, M., Karlstrom, L., & Wang, C.-Y. (2012). Mechanics of Old Faithful Geyser, Calistoga, California. *Geophysical Research Letters*, *39*(24). https://doi.org/10.1029/2012GL054012

Simioni, S., Dual, J., & Schweizer, J. (2017). Snowpack response to directed gas explosions on level ground. *Cold Regions Science and Technology*, *144*, 73–88. https://doi.org/10.1016/j.coldregions.2017.09.012

Smith, C. M., McNutt, S. R., & Thompson, G. (2016). Ground-coupled airwaves at Pavlof Volcano, Alaska, and their potential for eruption monitoring. *Bulletin of Volcanology*, *78*(52), 52. https://doi.org/10.1007/s00445-016-1045-0

Steinmann, R., Hadziioannou, C., & Larose, E. (2021). Effect of centimetric freezing of the near subsurface on Rayleigh and Love wave velocity in ambient seismic noise correlations. *Geophysical Journal International*, *224*(1), 626–636. https://doi.org/10.1093/gji/ggaa406

Taddeucci, J., Sesterhenn, J., Scarlato, P., Stampka, K., Del Bello, E., Pena Fernandez, J. J., & Gaudin, D. (2014). High-speed imaging, acoustic features, and aeroacoustic computations of jet noise from Strombolian (and Vulcanian) explosions. *Geophysical Research Letters*, *41*(9), 3096–3102. https://doi.org/10.1002/2014GL059925

Taylor, O. D. S., McKenna, M. H., Quinn, M. C., & Quinn, B. G. (2014). Partially saturated soil causing significant variability in near surface seismic signals. *Near Surface Geophysics*, *12*(4), 467–480. https://doi.org/10.3997/1873-0604.2013039

The ObsPy Development Team. (2020). ObsPy 1.2.2. [Software]. Zenodo. https://doi.org/10.5281/zenodo.3921997

University of Utah. (2021). Yellowstone National Park Seismograph Network. [Dataset]. International Federation of Digital Seismograph Networks. https://doi.org/10.7914/SN/WY

Vandemeulebrouck, J., Roux, P., & Cros, E. (2013). The plumbing of Old Faithful Geyser revealed by hydrothermal tremor. *Geophysical Research Letters*, *40*(10), 1989–1993. https://doi.org/10.1002/grl.50422

Vandemeulebrouck, J., Sohn, R. A., Rudolph, M. L., Hurwitz, S., Manga, M., Johnston, M. J. S., et al. (2014). Eruptions at Lone Star Geyser, Yellowstone National Park, USA: 2. Constraints on subsurface dynamics. *Journal of Geophysical Research: Solid Earth*, *119*(12), 8688–8707. https://doi.org/10.1002/2014JB011526

Vander Ley, B. (2021). Measuring the height of Steamboat Geyser in 2020, plus additional data. *The Geyser Gazer Sput*, *35*(2), 17–22.

Watson, L. M., Iezzi, A. M., Toney, L., Maher, S. P., Fee, D., McKee, K., et al. (2022). Volcano infrasound: Progress and future directions. *Bulletin of Volcanology*, *84*(44), 1–13. https://doi.org/10.1007/s00445-022-01544-w

White, D. E. (1967). Some principles of geyser activity, mainly from Steamboat Springs, Nevada. *American Journal of Science*, *265*(8), 641–684. https://doi.org/10.2475/ajs.265.8.641

Woulff, G., & McGetchin, T. R. (1976). Acoustic noise from volcanoes: Theory and experiment. *Geophysical Journal International*, *45*(3), 601–616. https://doi.org/10.1111/j.1365-246X.1976.tb06913.x

Wu, S.-M., Lin, F.-C., Farrell, J., & Allam, A. (2019). Imaging the deep subsurface plumbing of Old Faithful Geyser from low-frequency hydrothermal tremor migration. *Geophysical Research Letters*, *46*(13), 7315–7322. https://doi.org/10.1029/2018GL081771

Wu, S.-M., Lin, F.-C., Farrell, J., Keller, W. E., White, E. B., & Hungerford, J. D. G. (2021). Imaging the subsurface plumbing complex of Steamboat Geyser and Cistern Spring with hydrothermal tremor migration using seismic interferometry. *Journal of Geophysical Research: Solid Earth*, *126*(4), e2020JB021128. https://doi.org/10.1029/2020JB021128

Wu, S.-M., Ward, K. M., Farrell, J., Lin, F.-C., Karplus, M., & Smith, R. B. (2017). Anatomy of Old Faithful from subsurface seismic imaging of the Yellowstone Upper Geyser Basin. *Geophysical Research Letters*, *44*(20), 10240–10247. https://doi.org/10.1002/2017GL075255